11

Characteristics Study of 2DEG Transport Properties of AlGaN/GaN and AlGaAs/GaAs-based HEMT

© T.R. Lenka¶, A.K. Panda¶¶

National Institute of Science and Technology,
Palur Hills, Berhampur-761008, Odisha, India

(Получена 5 августа 2010 г. Принята к печати 2 ноября 2010 г.)

Growth of wide bandgap material over narrow bandgap material, results into a two dimensional electron gas (2DEG) at the heterointerface due to the conduction band discontinuity. In this paper the 2DEG transport properties of AlGaN/GaN-based high electron mobility transistor (HEMT) is discussed and its effect on various characteristics such as 2DEG density, $C-V$ characteristics and Sheet resistances for different mole fractions are presented. The obtained results are also compared with AlGaAs/GaAs-based HEMT for the same structural parameter as like AlGaN/GaN-based HEMT. The calculated results of electron sheet concentration as a function of the Al mole fraction are in excellent agreement with some experimental data available in the literature.

1. Introduction

High electron mobility transistor (HEMT) or modulation doped field effect transistor (MODFET) is the fastest transistor currently available and a suitable candidate for microwave and millimeter wave applications. It is heterostructure device and the unique properties of HEMT are a result of its use of bandgap engineering to create a two dimensional electron gas (2DEG) at the heterointerface [1]. Accumulation of the high density 2DEG is due to the formation of a deep spike-shaped quantum well at the heterojunction, where there is a large conduction-band offset as well as a large discontinuity in the piezoelectric and spontaneous polarization [2]. The fabrication process is very similar to MESFET and the conventional flow process includes following stages: growth of buffer layer, alternating layers, active channel, space layer and donor layer [2].

Here the authors have focused on GaN based devices due to its superior material properties over other existing counterparts such as GaAs, Si and Ge etc. Optimized AlGaN/GaN HEMTs play a vital role in the next generation 3G/4G mobile phone base stations, Wi-max, radar, mixers, oscillators, and attenuators in both commercial and military applications [3]. All these happen to possible due to its superior material properties such as high breakdown electric field (5 MV/cm), high thermal conductivity ($1.3\,\mathrm{Wcm^{-1}C^{-1}}$), high peak velocity ($> 3\cdot 10^7\,\mathrm{cm^{-1}s}$), high saturation velocity ($> 1.5\cdot 10^7\,\mathrm{cm^{-1}s}$), and high sheet charge density ($1\cdot 10^{13}\,\mathrm{cm^{-2}}$) [1–4]. Exploitation of these material properties and modern growth techniques lead the device to operate in microwave and millimeter wave applications [4–6].

For a successful design of advanced electronic devices based on AlGaN/GaN single heterojunction, it is necessary to analyze the polarization effects and to characterize the dependence of subband structures using available material parameters. However very less theoretical studies on 2DEG subbands in semiconductor heterostructures have been seen in the literature [1–20]. So the authors keep interest to understand the electrostatic behavior of GaN and GaAs based HEMTs and their potential usability. In this paper the 2DEG transport properties of the charge carriers of both devices are discussed, taking into account the piezoelectrical and spontaneous polarization and various subbands in the 2DEG.

The device structure, simulation and its physics are described in sect. 2. A basic formalism of the piezoelectric and spontaneous polarization in AlGaN/GaN heterojunction is discussed in sect. 3. 2DEG transport properties and its effect on various characteristics such as 2DEG density, sheet resistance for different mole fractions, $C-V$ characteristics in AlGaN/GaN and AlGaAs/GaAs devices are discussed in sect. 4. Apart from this a numerical method based on the effective mass approximation is described for subband calculations of AlGaN/GaN heterjunctions also discussed in this section and finally it is concluded in sect. 5.

2. Device structure and its simulation

The proposed device shown in Fig. 1 consists of a GaN substrate of thickness $0.8\,\mu$m and over which undoped AlGaN buffer layer is grown of thickness 100 Å followed by another doped layer of AlGaN of thickness $0.0345\,\mu$m. δ-doping has been done by introducing a sheet charge of $10^{12}\,\mathrm{cm^{-2}}$. The various structural parameters of the proposed device is enumerated in Table. AlGaN is a wide bandgap semiconductor of energy gap, $E_g = 4.24$ eV and GaN is a comparative less bandgap than AlGaN having energy gap, $E_g = 3.4$ eV. The growth of wide bandgap material over narrow band gap material creates a 2DEG in the heterointerface, so that confinement of electrons in the quantum well is possible, which leads to higher mobility and resulting into a high speed device.

Schrödinger's equation is solved self consistently with Poisson's equation in this device to find the electron concentration. Both heavy hole and light holes are

¶ E-mail: trlenka@gmail.com
¶¶ E-mail: akpanda62@hotmail.com

The structural parameters of HEMT

Parameter	Value
GaN substrate height	$0.8\,\mu$m
Height of AlGaN spacer	$0.0445\,\mu$m
Delta doping thickness	$0.002\,\mu$m
Height of GaN cap layer	$0.03\,\mu$m
Gate lendth (L_g)	$0.25\,\mu$m
Contact length (L_c)	$0.05\,\mu$m
Gate recess	$0.015\,\mu$m
Width of oxide spacer	$0.04\,\mu$m
Width of trap	$0.03\,\mu$m
Height of top passivation	$0.05\,\mu$m
Sheet charge	10^{12} cm^{-2}
x mole fraction ($Al_xGa_{1-x}N$)	0.3

considered in the simulation model [7,8]. Only one region of Schrödinger solution is allowed, and Boltzmann statistics is also used outside of the Schrödinger region. The Schrödinger solver finds bound subbands. In the specified region Schrödinger's wave equation is solved self-consistently with Poisson's equation and 2DEG is obtained. The recombination behaviors between electrons and holes are described with Auger's, Shockley–Read–Hall equations and direct-recombination equation [7,8]. From here $C-V$ analysis and microwave characteristics are also determined with our simulation technique where details are presented elsewhere [9]. We have considered the gate lengths of $0.25\,\mu$m and have simulated for a source, drain contact length of $0.05\,\mu$m. The Gate is of type Schottky-gate having work function of 0.9 eV considered in the simulation model. The polarization effects and based on this, the self-sonsistent numerical calculation for the subbands structure in 2DEG are presented in next sections.

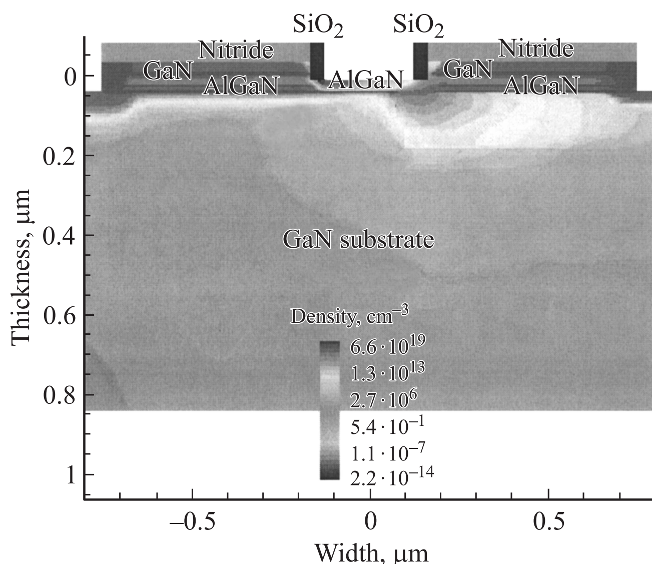

Fig. 1. GaN/GaN-based HEMT structure.

3. Polarization effects

AlGaN and GaN possess polarized Wurtzite crystal structures, having dipoles across the crystal in the [0001] direction as shown in Fig. 2. In the absence of external fields, this macroscopic polarization includes spontaneous (pyroelectric) and strain induced (piezoelectric) contributions [10–13]. The primary effect of polarization is an interface charge due to abrupt divergence in the polarization at the AlGaN/GaN heterointerface which is not seen in GaAs based devices.

In this work, it is assumed that GaN bulk is fully relaxed and, therefore, its polarization vector contains only the spontaneous component, P_{sp}(GaN). But for AlGaN layer, in addition to the spontaneous component P_{sp}(AlGaN), the piezopolarization component due to the presence of strain because of Al content in $Al_xGa_{1-x}N$ must be considered and is shown in Fig. 3. GaN and AlN values and linear interpolation are adopted in the computation of all mole fraction dependent piezoelectric and mechanical constants of AlGaN. The strain (ε) is computed using the in-plane

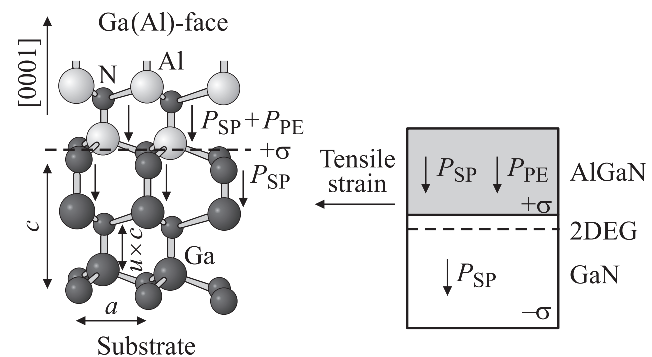

Fig. 2. Crystal structure and polarization effects (O. Ambacher et al [6]).

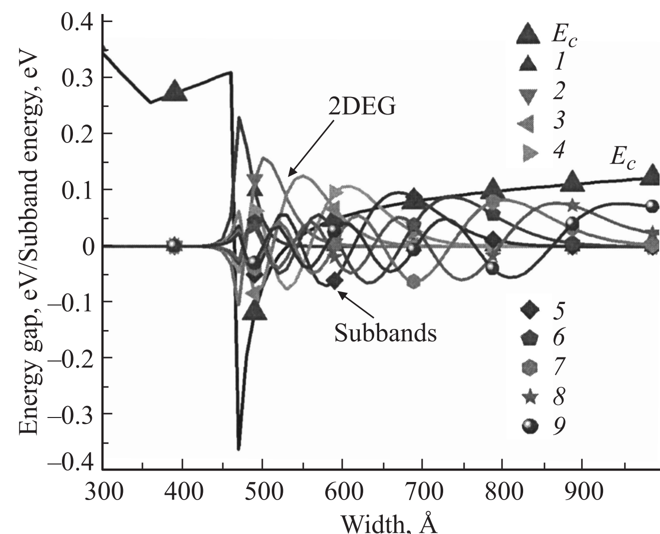

Fig. 3. 2DEG and subbands of AlGaN/GaN-based HEMT.

lattice constant, a, of GaN and AlGaN [10–13]:

$$\varepsilon = (1-r)\left(\frac{a_{\mathrm{AlGaN}} - a_{\mathrm{GaN}}}{a_{\mathrm{AlGaN}}}\right), \quad (1)$$

where a is the in-plane lattice constant and r is the amount of strain relaxation.

The piezopolarization component of AlGaN is given by [13]:

$$P_{\mathrm{pz}}(\mathrm{AlGaN}) = 2\varepsilon\left[e_{31} - e_{33}\left(\frac{c_{13}}{c_{33}}\right)\right]. \quad (2)$$

Therefore, the total polarization vectors for GaN and AlGaN are given by [13]:

$$P_{\mathrm{Tz}}(\mathrm{GaN}) = P_{\mathrm{sp}}(\mathrm{GaN}) + 0,$$

$$P_{\mathrm{Tz}}(\mathrm{AlGaN}) = P_{\mathrm{sp}}(\mathrm{AlGaN}) + P_{\mathrm{pz}}(\mathrm{AlGaN}). \quad (3)$$

The total heterointerface charges (σ) can be computed for the AlGaN surface and the AlGaN/GaN interface given as [13]:

$$\sigma_{\mathrm{surf}} = -\left[0 - P_{\mathrm{Tz}}(\mathrm{Al}_x\mathrm{Ga}_{1-x}\mathrm{N})\right], \quad (4)$$

$$\sigma(m) = \sigma_{\mathrm{AlGaN/GaN}}(x) = -\left[P_{\mathrm{Tz}}(\mathrm{Al}_x\mathrm{Ga}_{1-x}\mathrm{N}) - P_{\mathrm{Tz}}(\mathrm{GaN})\right], \quad (5)$$

where the total piezoelectric polarization of AlGaN layer is given as [13]:

$$P_{\mathrm{pz}}(\mathrm{Al}_x\mathrm{Ga}_{1-x}\mathrm{N}) = 2\left(\frac{\alpha(0) - \alpha(x)}{\alpha(x)}\right) \times \left[e_{31}(x) - e_{33}(x)\,\frac{c_{13}(x)}{c_{33}(x)}\right]\frac{C}{m^2}, \quad (6)$$

$$P_{\mathrm{sp}}(\mathrm{Al}_x\mathrm{Ga}_{1-x}\mathrm{N}) = -0.052x - 0.29\,\frac{C}{m^2}, \quad (7)$$

$$P_{\mathrm{sp}}(\mathrm{GaN}) = -0.029\,\frac{C}{m^2}, \quad (8)$$

where $\alpha(0)$ and $\alpha(x)$ are the lattice constants, $c_{13}(x)$ and $c_{33}(x)$ are the elastic constants and $e_{31}(x)$ and $e_{33}(x)$ are piezoelectric constants of AlGaN layer [13]. In the above expression, it has been assumed that GaN layer is fully relaxed. Thus $P_{\mathrm{pz}}(\mathrm{GaN})$ is almost zero.

The large polarization divergence at the $\mathrm{Al}_x\mathrm{Ga}_{1-x}\mathrm{N}$ barrier surface would completely deplete the channel of electrons, if not partially or completely compensated by positive charges. It is still not clear to the research community, whether the polarization charge is compensated by fixed charges or by interface trap states. Due to the relatively immature state of III-nitride technology, these materials tend to exhibit a significant number of structural defects, such as threading, misfit dislocations, and carbon impurities, which translate into bulk traps [8–13]. In this structure it's considered that all shallow dopants are ionized. The ionization of deep levels are also calculated.

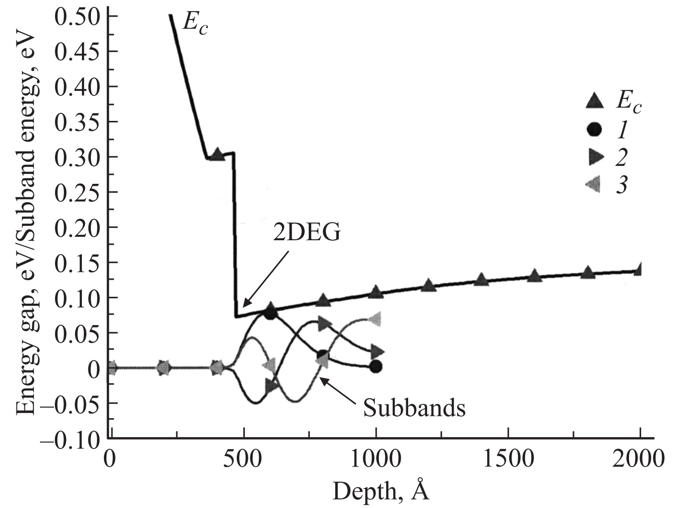

Fig. 4. 2DEG and subbands of AlGaAs/GaAs-based HEMT.

4. 2DEG transport properties

Two dimensional electron gas (2DEG) is also referred to as quantum well and it is formed at the heterointerface of wideband gap material, when it is grown over narrow band gap material. Here both AlGaN/GaN and AlGaAs/GaAs device is considered for their 2DEG transport analysis. This quantum well is formed at the heterointerface due to the conduction band discontinuity and has been realized by the TCAD device simulator and 1D Poisson solver. The growth of AlGaN material over GaN provides a unique polarization field such as spontaneous polarization and piezoelectric polarization, which results in a higher potential barrier at the backside of the 2DEG, and effectively improves the carrier confinement and then reduces the buffer leakage. These 2DEG's have been realized by solving Schrödinger's wave equation and Poisson's equation self consistently by both TCAD and 1D Poisson solver and are shown in Figs 3, 4 for GaN based and GaAs based HEMT's respectively.

4.1. Subband structure in 2DEG

In the effective mass approximation, the electronic subband states in the growth direction of a single heterojunction are solutions to the Schrödinger equation [14],

$$-\frac{\hbar^2}{2}\frac{d}{dz}\left[\frac{1}{m^*}\frac{d\psi_i(z)}{dz}\right] + [V(z) - E_i]\psi_i(z) = 0, \quad (9)$$

where m^*, $V(z)$, and E_i are the electron effective mass at the conduction-band edge, the potential energy, and the energy of the i-th subband, respectively. Ignoring the conduction-band non-parabolicity, we assume that m^* is independent of electron energy and has an isotropic value changing abruptly at the interface between the AlGaN and GaN. Here, we have used $m^* = 0.22m_0$ and $m^* = 0.242m_0$ for the GaN

and $Al_{0.3}Ga_{0.7}N$, respectively. $V(z)$ may be given as [14]

$$V(z) = V_c(z) + V_H(z) + V_{xc}(z), \quad (10)$$

where $V_c(z)$ represent the conduction-band edge potential in a form of the step-function associated with the conduction band offset at the AlGaN/GaN heterojunction, $V_H(z)$ is the Hartree potential of the electrostatic interaction due to mobile and immobile charges distributed in the system, and $V_{xc}(z)$ is the exchange-correlation potential representing the many-body interaction and not included in the $V_H(z)$ [14].

$V_H(z)$ is the solution to the Poisson equation,

$$\frac{d}{dz}\left[k(z)\frac{d}{dz}V_H(z)\right] = e^2\rho(z), \quad (11)$$

where k is the dielectric constant which is assumed to be changed abruptly at the AlGaN/GaN heterojunction. The density of total charges $\rho(z)$ is given as

$$\rho(z) = \sum_{j=t,i,b} \sigma(z)\delta(z-z_i) + p(z) + N_D^+(z) - n(z) - N_A^-(z), \quad (12)$$

where $\sigma(z)$, $p(z)$, N_D^+, $n(z)$ and N_A^- denote the density of immobile polarization charges, the density of free holes induced in the p-channels, the density of ionized donors, the density of free electrons in n-channels, and the density of ionized acceptors, respectively. From the neutrality condition, the following conditions must be satisfied for the sum of total charges:

$$\int_{z_t}^{z_b} \rho(z)dz = 0, \quad (13)$$

and for the sum of mobile charges:

$$\int_{z_t}^{z_b} \left[p(z) + N_D^+(z) - n(z) - N_A^-\right]dz = 0. \quad (14)$$

Considering AlGaN/GaN heterojunctions with a two dimensional electron-gas channel formed at the heterojunction, $n(z)$ is given as:

$$n(z) = \sum_i n_{s_i}|\psi_i(z)|^2, \quad (15)$$

where n_{s_i} is the sheet density of electrons in the ith subband and is given by as a function of effective mass,

$$n_{s_i} = \frac{m^* k_B T}{\pi\hbar^2}\ln\left[1 + \exp\left(\frac{E_F - E_i}{k_B T}\right)\right]. \quad (16)$$

Here, k_B and T are the Boltzmann constant and the electron temperature, respectively. The Fermi energy E_F is determined from the condition that the sum of subband electron densities is equal to the total electron density N_e:

$$N_e = \int_{z_t}^{z_b} n(z)dz = \sum_i n_{s_i}. \quad (17)$$

N_e can be determined in a self-consistent manner using two boundary conditions for Fermi-level pinning at the upper and the lower boundaries of the system [14].

The various subband energies are computed and is realized that they originate at the AlGaN/GaN heterointerface, where 2DEG is formed and shown in Fig. 3. The subbands are restricted from -0.1 to 0.25 eV. Alternatively there is little wave function penetration into the AlGaN barrier, which is called quantum effect, seen in the structure [14]. The 2DEG in case of GaN based HEMT is very sharp and the conduction discontinuity is larger than 0.6 eV for Al mole fraction of $x = 0.3$.

4.2. AlGaN/GaN-based HEMT

The 2DEG density of the AlGaN/GaN based HEMT can be written as [15]

$$n_s = \frac{\sigma_{AlGaN}t_{AlGaN} - \frac{\varepsilon\varepsilon_0}{q}\phi_B + \frac{\varepsilon\varepsilon_0}{q^2}(\Delta E_{c,AlGaN})}{t_{AlGaN} + d_0}, \quad (18)$$

where n_s is the 2DEG density shown in Fig. 5, σ_{AlGaN} is the net polarization charge density of AlGaN, $\Delta E_{c,AlGaN}$ is the conduction band discontinuity, t_{AlGaN} is thickness of AlGaN layer and the conduction band discontinuity $\Delta E_{c,AlGaN}$ in this $Al_{0.3}Ga_{0.7}N$/GaN is about approximately 0.6 eV and is shown in Fig. 3.

But increasing the product of $n_s\mu_n$ is critical to obtaining high power density. Moreover, in applications such as power switching, a high $n_s\mu_n$ product is also desirable as it is inversely proportional to on-resistance for the device, which is a key figure of merit for power switching devices [16].

From Eq. (19), the $n_s\mu_n$ product represents the conductivity of the 2DEG. Often the sheet resistance extracted from Hall measurements is used to evaluate this property. The sheet resistance of the device is reported to be $148\,\Omega/\Box$ and the 2DEG density is reported to be $1.2 \cdot 10^{14}\,\text{cm}^{-2}$ and is of good agreement with Eq. (19)

$$R_{sheet} = \frac{1}{qn_s\mu_n}. \quad (19)$$

The relationship between n_s and μ_n has to be considered, when optimizing the $n_s\mu_n$ product. For example, it is well-known that increasing the Al mole fraction of AlGaN barrier can increase 2DEG density. In an AlGaN/GaN HEMT, the 2DEG sheet charge density approaches the net polarization charge density at AlGaN/GaN interface with increasing AlGaN thickness. The polarization charge density increases in turn with Al mole traction of the AlGaN barrier.

4.3. AlGaAs/GaAs-based HEMT

The 2DEG for AlGaAs/GaAs based HEMT is formed due to the growth of wide bandgap AlGaAs over, narrow bandgap GaAs material and is shown in Fig. 4. The 2DEG is comparatively not so sharp like GaN based HEMT. The subbands are restricted from -0.05 to 0.1 eV.

The 2DEG density with the variation of gate voltage from -4 to $+4$ V, at different mole fractions from $x = 0.2$ to $x = 0.45$, for AlGaN/GaN based and AlGaAs/GaAs based

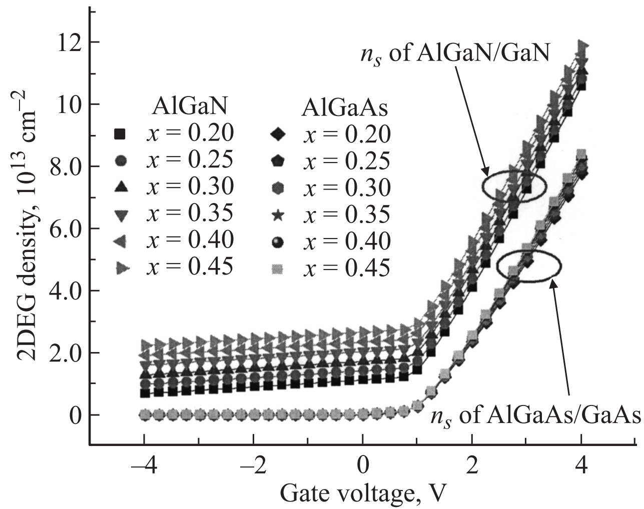

Fig. 5. 2DEG density of AlGaN- and AlGaAs-based HEMT for different mole fractions.

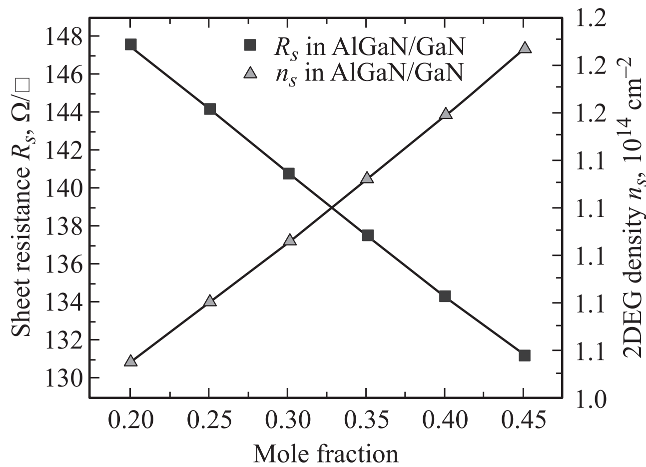

Fig. 6. Sheet resistance and 2DEG mobility of AlGaN/GaN-based HEMT for different mole fractions.

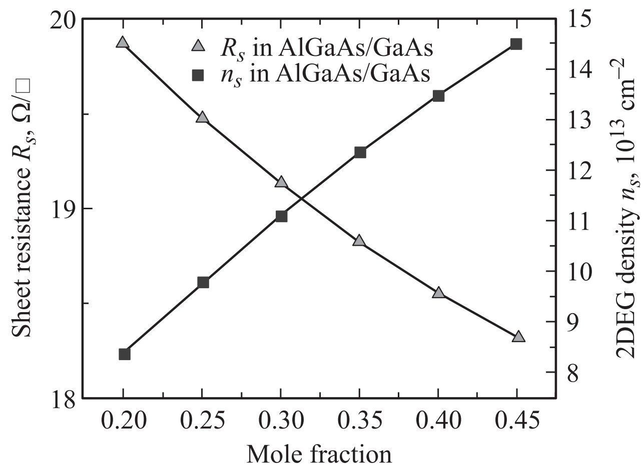

Fig. 7. Sheet resistance and 2DEG density of AlGaAs/GaAs-based HEMT for different mole fractions.

devices are computed and are shown in Fig. 5. It is interesting to be noted from the figure that the 2DEG density for GaN based devices reach to a peak point of $1.2 \cdot 10^{14}$ cm^{-2} at a gate voltage of 4 V, where as for GaAs based devices the 2DEG density reaches to a peak of $8 \cdot 10^{13}$ cm^{-2}. It is also seen from the 2DEG profile that as the Al mole fraction increases the 2DEG density also increases with the gate voltage for both types of devices. Therefore AlGaN based HEMTs are quite advantageous over its counterparts due to strong polarization effects resulting into high 2DEG density.

The sheet resistance and 2DEG density of AlGaN/GaN and AlGaAs/GaAs HEMTs for different mole fractions are presented in Figs 6, 7 respectively and is given by Eq. (19). It is noteworthy to mark that the sheet resistance of AlGaN/GaN HEMT is decreasing from 148 Ω/□ at $x = 0.2$ to 131 Ω/□ at $x = 0.45$. But for AlGaAs/GaAs HEMT the sheet resistance is decreasing from 20 Ω/□ at $x = 0.2$ to 18 Ω/□ at $x = 0.45$.

As mole fraction increases from 0.2 to 0.45, the 2DEG density increases to an order of 10^{14} and 10^{13} cm^{-2} in case of AlGaN/GaN HEMT and AlGaAs/GaAs HEMT and are shown in Figs 6, 7 respectively. The calculated results of electron sheet concentration as a function of the Al mole fraction are in excellent agreement with some experimental data available in the literature [17–19].

5. $C-V$ characteristics

The capacitance-voltage characteristics of the lattice mismatched $Al_xGa_{1-x}N$/GaN based HEMTs are obtained using charge controlled analysis for its microwave performance [20]. The model includes the spontaneous and piezoelectric polarization effects to calculate capacitances and it is mainly due to the formation of 2DEG in the heterojunction of $Al_xGa_{1-x}N$/GaN layer [20]. The $C-V$ analysis has been done with the help of small signal model in a mixed-mode environment. The major parasitic capacitance includes gate-to-source and gate-to-drain capacitances.

The capacitance with the variation of gate voltage from -4 to $+4$ V, for different mole fractions from $x = 0.2$ to $x = 0.45$, for AlGaN/GaN based and AlGaAs/GaAs based devices are computed and are shown in Fig. 8. As gate voltage increases upto 4 V, the capacitance for AlGaN based HEMT increases upto a peak value of $5.5\,\mu$F/cm^2. But in case of AlGaAs based HEMT, the capacitance increases upto a maximum peak value of $5\,\mu$F/cm^2. But for different mole fractions there is little significant change in the capacitance of both devices. As per the $C-V$ profile shown in Fig. 8, the gate capcitance of the structure is maintained to be a very small value upto a gate voltage of 1 V, because the 2DEG density is also maintained to be constant (little increase) upto a gate voltage of 1 V.

The mobility variation with gate voltage from -4 to 4 V in AlGaN/GaN HEMT is shown in Fig. 9 for different mole fractions. The mobility is around 6160 cm^2/(V · s) for $x = 0.2$ at low voltage. But when gate voltage increases

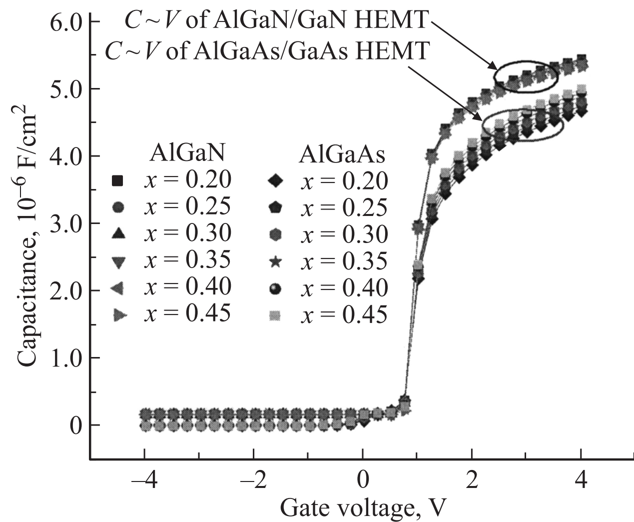

Fig. 8. $C-V$ characteristics of AlGaN- and AlGaAs-based HEMT for different mole fractions.

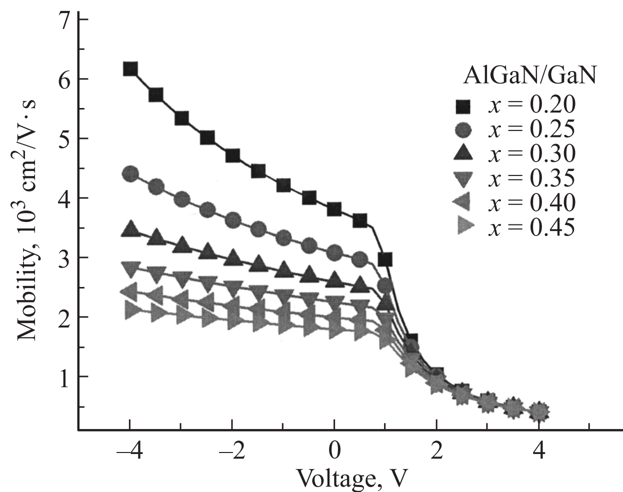

Fig. 9. Mobility with gate voltage variation of AlGaN/GaN HEMT.

upto 4 V then the mobility decreases to $420\,\text{cm}^2/(\text{V}\cdot\text{s})$. It's depicted in the Fig. 6, 7 that as mole fraction increases, the 2DEG density increases sharply but in case of mobility is concerned it decreases due to the introduction of many scattering mechanisms such as alloy, phonon, ionized impurity scattering, which are not discussed here.

6. Conclusion

Similar structure of HEMT is considered for GaN- and GaAs-based HEMT to understand the electrostatic behavior and 2DEG transport properties and its effect on 2DEG density, $C-V$ characteristics and sheet resistance. Change of Al mole fraction enhances the 2DEG density greatly for a AlGaN/GaN-based HEMT rather AlGaAs/GaAs-based HEMT because of reducing the electon wave function penetration into the AlGaN barrier layer and the larger effective ΔE_c also increased the 2DEG density. The conduction-band profile and subband structure of $\text{Al}_x\text{Ga}_{1-x}\text{N}$/GaN heterojunction are calculated by a self-consistent numerical method and resulting into a shrp 2DEG. Piezoelectric and spontaneous polarization, significantly affect the subband structure of $\text{Al}_x\text{Ga}_{1-x}\text{N}$/GaN heterojunction rether $\text{Al}_x\text{Ga}_{1-x}\text{As}$/GaAs heterojunction. More gate capacitance upto $6\,\mu\text{F/cm}^{-2}$ is achieved for AlGaN/GaN-based HEMT rather approximately $5\,\mu\text{F/cm}^{-2}$ for AlGaAs/GaAs HEMT. The 2DEG sheet concentration at the $\text{Al}_x\text{Ga}_{1-x}\text{N}$/GaN heterojunction is sensitively dependent on the Al mole fraction, which leads the GaN-based HEMT, towards microwave and millimeter wave applications.

The authors acknowledge the DST-FIST fund received by National Institute of Science and Technology from Department of Science & Technology (DST), Government of India.

References

[1] M.A. Huque, S.A. Eliza, T. Rahman, H.F. Huq, S.K. Islam. Sol. St. Electron., **53**, 341 (2009).
[2] Rashmi et al. IEEE Trans. Microwave Theory and Techniques, **51** (2), 607 (2003).
[3] A.K. Panda, D. Pavlidis, E. Alekseev. IEEE Trans. Electron. Dev., ED-**48** (4), 820 (2001).
[4] T. Palacios et al. IEEE Electron. Dev. Lett., **26**, 781 (2005).
[5] Synopsys User Guide Manuals (2007).
[6] Y. Ando et al. IEEE Electron. Dev. Lett., **24** (5), 240 (2003).
[7] J.C. Lin, P.Y. Yang, W.C. Tsai. Microelectronics J., **38**, 251 (2007).
[8] A. Brannick, N.A. Zakhleniuk, B.K. Ridley, L.F. Eastman, J.R. Shealy, W.J. Schaff. Microelectronics J., **40**, 410 (2009).
[9] T.R. Lenka, A.K. Panda. *Proc. 15th IWPSD* (2009) p. 117.
[10] R.J. Trew. In: *Int. Semicond. Dev. Res. Symp.* (Dec. 5–7, 2001) p. 432.
[11] L. Shen et al. IEEE Electron. Dev. Lett., **22** (10), 1200 (2001).
[12] P. Gangwani et al. Sol. St. Electron., **51**, 130 (2007).
[13] O. Ambacher et al. J. Appl. Phys., **87** (1), 334 (2000).
[14] Kyu-Seok Lee, Doo-Hyeb Yoon, Sung-Bum Bae, Mi-Ran Park, Gil-Ho Kim. ETRI J., **24** (4), 270 (2002).
[15] S. Milshtein, A. Churi, C. Gil. Microelectronics J., **40**, 554 (2009).
[16] Jing Lu et al. Sol. St. Electron., **52**, 115 (2008).
[17] Y. Zhang, I.P. Smorchkova, C.R. Elsass, S. Keller, J.P. Ibbetson, S. DenBaars, U.K. Mishra, J. Singh. J. Appl. Phys., **87**, 7981 (2000).
[18] I.P. Smorchkova, S. Keller, S. Heikman, B. Heying, P. Fini, J.S. Speck, U.K. Mishra. Appl. Phys. Lett., **77** (24), 3998 (2000).
[19] I.P. Smorchkova, L. Chen, T. Mates, L. Shen, S. Heikman, B. Moran, S. Keller, S.P. DenBaars, J.S. Speck, U.K. Mishra. J. Appl. Phys., **90** (10), 5196 (2001).
[20] P. Gangwani et al. Microelectronics J., **38**, 848 (2007).

Редактор Т.А. Полянская